A CALCULATION METHOD FOR OVER-THE-WING ENGINES WITHIN CONCEPTUAL AIRCRAFT DESIGN

M. Nuño[1], M.Y. Pereda Albarrán[2], E. Dincer[3], K.-U. Schröder[1], E. Stumpf[2];
[1]Institut für Strukturmechanik und Leichtbau, RWTH Aachen University, DE ;[2]Institut für Luft- und Raumfahrtsysteme, RWTH Aachen University, DE; [3]RWTH Aachen University, DE

Abstract

In this paper, a physics-based computationally inexpensive model is developed to predict aircraft performance variation due to over-the-wing engine installation effects in terms of lift, drag and structure weight at the conceptual stage of aircraft design. The aerodynamic influence caused by the installation of the engine is calculated at cruise conditions using a vortex lattice method. The structural wing weight is calculated iteratively by means of inner loads considering aerodynamic loads, inertial loads and engine thrust. After a parameter study, formulas which can be used to take into account the position of over-the-wing engines during conceptual aircraft design are developed.

1. INTRODUCTION

The design of a revolutionary new generation of eco-friendly aircraft is crucial to diminish the negative consequences of the expected global air traffic growth [1]. Since the last decades, the aircraft basic configuration has not experienced major modifications after the establishment of the classical tube-and-wing aircraft configuration with under-the-wing mounted engines. One aircraft design approach, that could effectively reduce noise, and simultaneously addresses the integration challenge of larger fan diameters of modern high, or even ultra-high, bypass ratio engines, is to mount the engines above the wing [2]. Despite some older aircraft, like the VFW-Fokker 614, or very actual, such as the HondaJet HA-420, to mount the engines in pods on pylons above the wing, it is not a widespread practice. Consequently, comprehensive data, based in the experience gained by other aircraft designs, is insufficient and thus inexpensive physic-based calculation methods, appropriate for conceptual aircraft design, are missing so far. The aim of this study is to save this gap and provide the conceptual aircraft designer with the required tools and analysis methods to quickly estimate how the positioning of the engines above the wing modifies the aircraft design and performance.

To do so, a multidisciplinary approach accounting with the cooperation of two RWTH Aachen University institutes, has utilized the detailed results obtained by the Aircraft Structural Design Tool (ASDT) developed at the Institute of Structural Mechanics and Lightweight Design to assess the local impact of the engine position in terms of mass and aerodynamic performance on the aircraft wing, and thus in the complete aircraft design. The obtained results are integrated in the Multidisciplinary Conceptual Aircraft Design and Optimization environment (MICADO), from the Institute of Aerospace Systems, which can capture the impact of design changes on overall aircraft level, including mass snowball effects and resizing of main aircraft components.

2. FUNDAMENTALS FOR THE DESIGN OF OVER-THE-WING ENGINE AIRCRAFT

Among the reasons that might lead an aircraft designer to select an over-the-wing engine configuration for a future airliner, stands out the increased noise shielding. Noise shielding consists of placing a barrier between the engines and the ground by means of the aircraft wings and/or tailplane, which can effectively block and deflect the sound rays emitted by the fan reaching the observers [3, 4]. On the other hand, jet noise is particularly difficult to shield because it is a distributed source downstream of the engine exhaust [5]. Despite this, the overall noise signature of advanced turbofan engines with highly loaded, wide chord fan blades is dominated by fan discharge noise [6]. Modern, high pressure cores and high bypass ratio cycles extract significant energy from the core air flow, which tends to reduce primary jet noise. This contrasts with older technology engines, where jet noise is prominent and fan inlet noise is at least as high as fan discharge noise [7]. In this sense, noise shielding relative importance is increasing for actual and future engines. Also, flow interaction between engine exhaust and the trailing-edge devices is an important source of noise [8]. The positioning of the engines above the wing practically eliminates these effects and also removes the need for thrust gates in the flap system. Gaps of any kind reduce lift, increase drag and enhance the design complexity. In addition, the flaps can be deployed to higher angles without encountering the high dynamic pressures and temperatures of the exhaust gases of the engine. On the other hand, the Coanda effect can cause the high temperature exhaust gases to remain attached to the flap upper surface [9].

Due to the increased ground clearance, higher bypass ratios are easily realizable for over-the-wing engine configurations with a consequent improved fuel burn and emissions reductions [10]. Consequently long, and thus heavier, landing gears can dispense with, as well as high-wings. This engine position not only provides adequate ground clearance for nacelle strike but also improves safety in the unlikely event of a wheels-up landing or water ditching. Furthermore, the likelihood of foreign object ingestion damage is significantly reduced [11].

doi:10.25967/480177

Placing the engine over the wing is often considered as aerodynamically unfavorable since the airflow is disturbed on the wing upper side, where the most amount of lift is created. While in cruise, the nacelles can induce a strong shock wave resulting in a lower drag-divergence Mach number.

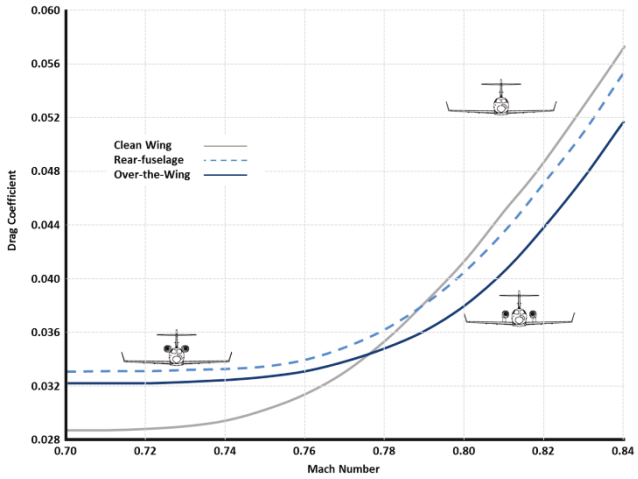

Figure 1: *Comparison of drag divergence for various nacelle configurations.*

However, as it can be observed in *Figure 1* promising results during the design of the HondaJet were obtained. If the nacelle is located at the optimum position relative to the wing, the shock wave can be minimized, leading to higher drag divergence Mach numbers when compared to the clean-wing configuration. Theoretical analyses and experimental measurements demonstrate that a wave-drag reduction can be achieved by locating the nacelle front face near the shock-wave position on the wing. The vertical distance between the wing and the nacelle should be about one third to one half of the maximum height of the nacelle. For this nacelle location adding a pylon improves the drag-divergence characteristics, and a contoured pylon, aligned with the local flow, improves the aerodynamic interference at lower Mach numbers. This over-the-wing nacelle configuration reduces the cruise drag at transonic speeds without altering the original geometry of the natural-laminar-flow wing [12].This analysis is far beyond the scope of aircraft conceptual design and thus the aerodynamic design in this paper concentrates just on how the aerodynamic interference between nacelles and pylons with the wing by using a vortex-lattice method.

The flight mechanics of the aircraft are also modified. The pitching-moment coefficient of the over-the-wing nacelle configuration is less positive, or even negative depending on the z position of the aircraft center of gravity, than those of the under-the-wing engine or clean-wing configuration. Therefore, less download on the horizontal tail is required to trim the airplane, reducing the download on the horizontal tail, leading to lower trim drag [12]. Also, the stall characteristics are improved for over-the-wing mounted engines. According to the standard recovery procedures of an incipient stall, the angle of attack must be reduced and full thrust must be applied. The pitching-up moment caused while increasing thrust to recover from a primary incipient stall can be so decisive that a secondary stall might occur despite correct pilot action for engine under-the-wing aircraft, especially with high thrust-to-weight ratios aircraft. This disadvantage is solved by placing the engines over the wing.

The aerolastic modelling and analysis of the wing-engine system is of particular interest, especially when positioning the engine behind the elastic axis of the wing, which decreases flutter speed [13]. Complex wing flutter characteristics can arise from this configuration leading to significant changes on the vibration modes of the original wing. The location of the engine mass and the stiffness of the pylon relative to the wing are important in preventing hazardous wing flutter. In addition, aerodynamic interference between the wing and the nacelle may cause unfavorable flutter characteristics, in particular, at transonic speeds [14]. In this paper, only static loads are taken into account to dimension the wing structure. Models of the clean wing and the wing-engine system are compared and effects of chordwise, spanwise locations and relative height above the upper surface of the wing are analyzed. The detailed flutter characteristic of the wing/engine systems are out of the scope of conceptual aircraft design.

Ideal conditions for the operation of the engine are a steady, continuous flow of air. However, at high angles of attack and/or sideslip angles for over-the-wing engine-mount configuration, the inlet-flow can suffer from important inlet-flow distortions. These flow distortions can lead to instabilities in the fan, leading to performance reduction and increased noise. An investigation for the HondaJet was conducted to determine if the measured total-pressure distortion exceeded the limits for high and low mass-flow conditions at various angles of attack and sideslip angles. The inlet total-pressure distortion was less than 0.1% up to the stall angle of attack and less than 2% at post stall angles of attack. Similar tendencies were obtained from tests with low and high mass-flow ratios. The results demonstrated that the distortion did not exceed the limits specified by engine requirements within the flight envelope. Furthermore the over-the-wing configuration has higher cruise efficiency than that of a conventional rear-fuselage engine-nacelle configuration due to clearer inlet flow of air [15]. Also, by mounting the engines on the wings, the carry-through structure required to mount the engines on the rear fuselage is eliminated. This would allow the fuselage internal space to be maximized without increasing its size [16].

3. ADAPTION OF MICADO FOR ENGINE-OVER-THE-WING AIRCRAFT

A detailed description of MICADO is given in Ref. [17]. The integrated sizing approach allows capturing the impact of particular design changes or the integration of innovative systems and technologies on overall aircraft level, including mass snowball effects and resizing of main aircraft components. MICADO has already been used for several applications in aircraft design and operational studies as well as systems and technology integration and assessment (e.g., see Ref. [18, 19]). In the following, as already explained in [20], only the main aspects of MICADO, which are relevant for this paper, are described. In the MICADO aircraft design process, the different aircraft components are sized and located with respect to the specified top-level aircraft requirements (TLARs). For the initial aircraft geometry, aerodynamic characteristics as well as component and system masses are predicted. A detailed mission simulation model [21], which uses the aircraft

mass, flight configuration dependent drag polars and engine performance decks, can accurately calculate the block fuel required on the aircraft design mission. All sizing and analysis programs are re-executed until convergence in key design parameters (e.g. maximum takeoff weight (MTOW), block fuel) is achieved, where wing loading W/S and thrust-to-weight ratio T/W are kept constant during design iteration. The fully converged aircraft design can then be assessed and optimized towards selected evaluation parameters, e.g., block fuel on a study mission, costs, emissions or noise.

For aircraft configurations with Engines-under-the-Wing (EuW) and conventional empennage, the engines and nacelles are sized according to the required sea-level static thrust. The effects of propulsion integration location are considered in terms of calculation of the structural mass of the wing and fuselage, as well as estimation of component drag. However, the influence of the propulsion location to the lift-distribution of the wing is neglected within the aerodynamic tool of MICADO. To estimate the lift produced by the aircraft lifting surfaces (wing and horizontal tailplane) the DLR tool LIFTING_LINE [22] is utilized. The current LIFTING_LINE version 2.5 is not capable to calculate the interference with the propulsion system. This is not of relevance as long as only EuW-configurations or configurations with engines on the fuselage are designed since the expected interference with the lift creation remains small. Nevertheless, it becomes more meaningful if EoW-configurations are examined as within this paper. For structural wing mass estimation a “quasi-FEM” method is applied using a beam-model of the wing with point loads for propulsion group and landing gear group, as well as section load for the lift-distribution [23]. The EoW-configuration has no effect on the structural wing weight so far.

To address this problem, the requirements for a short-range reference aircraft have been used in this paper. The “Central Reference Aircraft data System (CeRAS)” [24, 25] from the aircraft CSR-01, a central reference aircraft for research with conventional wing as well as empennage configuration is selected. The aircraft was designed for a range of 2500 NM and a payload of 17 000 kg with the ILR design platform MICADO. It is powered by two under-the-wing-mounted V2527-A5 turbofan engines with a sea-level static thrust of 117.88 kN each. For this paper solely the weight is changed to a maximum takeoff weight of 73 500 kg, resulting in a derivative of the CSR-01 named ILR-01 in the scope of this paper. The outer geometry of ILR-01 remains constant compared to the CSR-01 to be able to compare both designs. This results automatically in a lower wing loading and higher thrust-to-weight, respectively. The resulting key aircraft characteristics of the ILR-01 are summarized in **Table 1**.

Parameter	Symbol	Unit	CSR-01	ILR-01
Design Range	R	NM	2500	
Design passenger capacity	-	PAX	150	
Design payload	PL	kg	17 000	15 316.5
Cruise Mach number	M_{Cr}	-	0.78	
Wing-loading	W/S	kg/m²	629.1	600.5
Thrust-to-weight ratio	T/W	-	0.312	0.327
Maximum takeoff weight	MTOW	kg	77 000	73 500
Operating weight empty	OWE	kg	42 100	
Wing area	S_{ref}	m²	122.4	
Wing span	b	m	34.1	
Mean aerodynamic chord	MAC	m	4.2	
Engine type	-	-	2 x V2527-A5	
Sea-level static thrust	SLST	kN	117.88	
Block fuel @ design mission	BF_{DM}	kg	14 789	13 109

Table 1: *Comparison of Key Aircraft Characteristics of ILR-01 with CSR-01*

Parameter	Symbol	Unit	ILR-01	ILR-01T
Configuration	-	-	Convent.	T-tail
Horizontal tailplane				
Aspect ratio	Λ_{HTP}	-	5	4.7
Taper ratio	λ_{HTP}	-	0.38	0.31
Reference area	$S_{ref,HTP}$	m²	35.95	26.2
Vertical tailplane				
Aspect ratio	Λ_{VTP}	-	1.89	0.95
Taper ratio	λ_{VTP}	-	0.4	0.39
Reference area	$S_{ref,VTP}$	m²	27.97	27.03

Table 2: *Comparison of tail geometry for ILR-01 and ILR-01T.*

Starting from this baseline configuration a configuration with EoW has to be derived. This is done in two steps. When placing the engines over the wing, it is necessary to keep the tailplane well out of the exhaust gases of the engine. Considering this requirement, a T-tail empennage configuration might be an appropriate solution [26]. Therefore, as previous step before placing the engines over the wing, it is necessary to assure that any performance modification caused by this configurational variation does not mask the effect of placing the engines over the wing. This is why the initial derivative of the ILR-01 is a configuration using a T-tail, named ILR-01T. All other design specifications are kept constant. **Table 2** illustrates the change in geometry parameters of the empennage if the

ILR-01 is designed in T-tail configuration instead of conventional configuration. The overall geometry parameters of the empennage are in an accurate range for conventional short-range aircraft and the changes, especially in the aspect ratio between the conventional vertical tail and T-tail, have correct tendencies. Due to a smaller empennage in terms of reference area for horizontal and vertical tail, there is a slight reduction in the structural mass of the empennage in T-tail configuration (~12% for the HTP and ~5% for the VTP). The calculation method does not include the structural modification of the VTP, which in case of T-tail has to carry the loads from the HTP. In consequence, even with smaller areas the T-tail should be heavier. On the overall operating weight empty, this small reduction has a negligible influence. Regarding the aerodynamics, the smaller area entails a slight drag reduction in viscous drag. The induced drag component is increasing due to an increase in the lift coefficient required for the main wing. This leads to an overall drag increase summed up in a small reduction of aerodynamic performance in terms of L/D. Combined with the decrease in OWE the ILR-01T needs 100 kg more fuel to fulfill the same design mission. In conclusion, all main aerodynamic and mass effects are below 1% so that there is no major effect to the overall aircraft performance of the ILR-01T due to the configuration change [20]. The exterior geometry of the different aircraft developed in this study are presented in Figure 2.

Starting from the ILR-01T, the engines are placed over-the-wing (EoW) leading to a family of aircraft, the ILR-01EoW, where the engine position will be iteratively varied.

Figure 2: *From left to right: ILR-01, ILR-01T, and ILR-01EoW.*

For placing the engines over the wing, a new pylon design method is developed. A detailed method explanation can be found in Section 5.

To estimate the aircraft performance modification due to the engine position in terms of aerodynamic performance and structural mass with higher precision, the ASDT tool is utilized. A detailed explanation of the structural design can be found in Section 4. For the aerodynamic performance calculation, wave drag and viscous drag are calculated in MICADO and assumed to be independent on the engines position. Induced drag is calculated with AVL for every configuration.

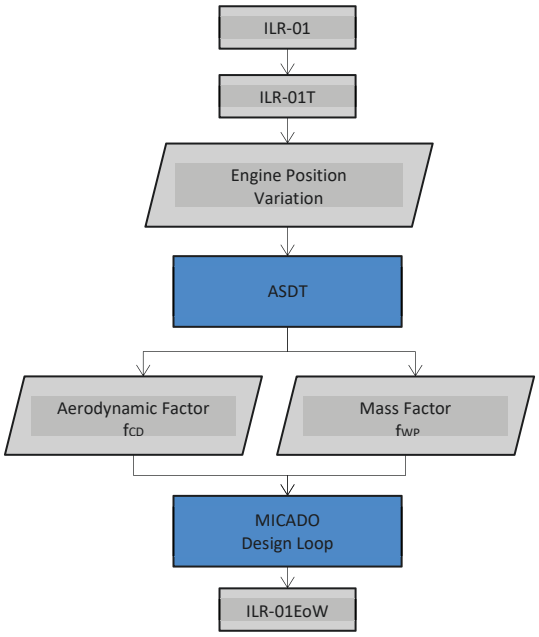

Figure 3: *Over-the-wing aircraft design process*

As it is not possible to integrate the ASDT environment directly into the MICADO toolchain, correction factors for the structural mass, wing and pylon, f_{WP} and aerodynamic performance, drag coefficient, f_{CD} are calculated based on the engine position. The definition of both factors can be found in Equation 1 and 2. Both factors are added to the MICADO design loop, so snowball effects throughout the iterative design process are modelled.

$$(1) \qquad f_{WP} = \frac{m_{W,EoW} + m_{P,EoW}}{m_{W,EuW} + m_{P,EuW}}$$

$$(2) \qquad f_{Cd} = \frac{C_{d,EoW}}{C_{d,EuW}}$$

The complete process is schematically presented in **Figure 3**. The detailed calculation of these factors is explained in detail in Section 6.2.

4. AIRCRAFT STRUCTURAL DESIGN TOOL

The ASDT is a Toolbox written in MATLAB used for preliminary structural design. The design is driven by the aircraft geometry, predefined load cases, section topologies as well as chosen materials. This approach, based on a simple beam model, makes it possible to estimate the structural masses of unconventional aircraft configurations, like the ones with over-the-wing engines presented in this paper, where almost no empirical data is available. Such an approach has already been employed in several cases like achieving good results [27, 28]. The structural design is performed in the following steps:

1. Load aircraft data from the MICADO xml-File
2. Calculate aerodynamic loads according to some predefined load cases
3. Discretize the structure in sections and create a stick beam structural model.
4. Structural optimization until mass convergence is achieved:
   i. Calculation of mass loads
   ii. Calculation of the inner loads at each section
   iii. For each section, sizing of the wingbox according to the calculated inner loads
   iv. Calculation of wing masses

4.1. Wing discretization

To perform the sizing, the wing is discretized in 49 sections, with a beam between each section. The total mass of the wing is calculated adding the masses of all beams. The mass of each beam is calculated multiplying its length with the averaged linear mass of the neighboring sections and a factor to take non-structural masses into account.

4.2. Loads calculation

For the wing mass estimation, the following symmetrical load cases (LC) are assumed to be critical and can be found in **Table 3**.

LC	Description	n [-]	Thrust [kN]
1	V_A pullup at T_{SLST}	2.5	112.2
2	V_A pullup at T_{cruise}	2.5	21.7

Table 3: *Structure design critical load cases.*

To calculate the inner loads of the wing, aerodynamic and mass loads as well as engine thrust are taken into account. Ultimate loads, used to size the structure, are calculated using a factor of 1.5.

Aerodynamic loads are calculated using AVL 3.36. AVL is an aerodynamics calculation program for rigid aircraft which uses an extended vortex lattice method [29]. Vortex lattice methods can be used to calculate the lift distribution on swept wings while being faster and easier to set up than Navier-Stokes based CFD codes. Non-induced drag loads cannot be calculated with a vortex lattice method. However, drag is usually one to two orders of magnitude smaller than lift and has therefore a small influence on the load carrying structure. The influence of the engine position on the wing lift is, to a certain degree, modelled by the vortex lattice method. These factors make AVL well-suited for calculations in the preliminary design stage. In **Figure 4** the basic model of the wing structure used in AVL can be seen.

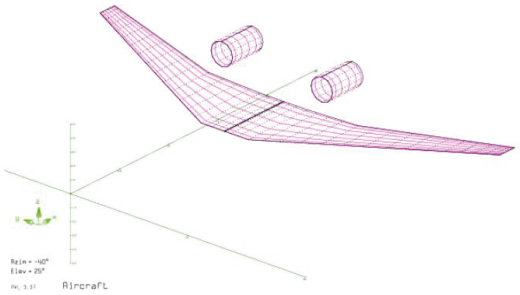

Figure 4: *Aerodynamic calculation of a random over-the-wing engine geometry.*

The discretized wing, as well as the engines, are modelled as point masses. Inertial loads acting on each point mass are calculated multiplying its mass with the corresponding total load factor.

Inner loads at each section are calculated with a force equilibrium on the rigid aircraft, taking into account all forces and moments outboard the corresponding section. The inner forces are referenced around the center of the wingbox, which corresponds to both the elastic and tension axis. The centroid of each section is also assumed to lay on the center of the wingbox

4.3. Wingbox sizing

The wingbox is assumed to be a thin-walled rectangular profile, with a height h and width b. The thickness of the webs is p_1, the caps thickness is p_2. A schematic of the profile can be seen in **Figure 5**.

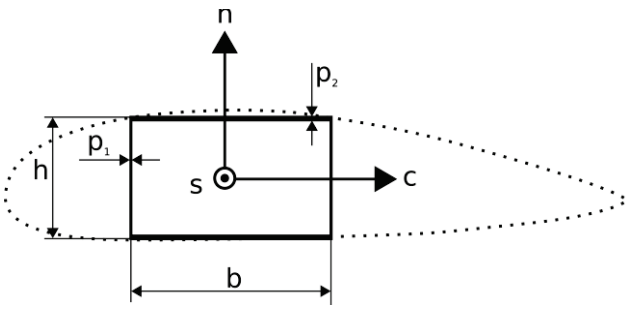

Figure 5: *Wingbox geometry*

The height h at each section is calculated averaging the airfoil thickness at the webs of the wingbox. The width b corresponds to the distance between the webs, which are placed at 18% and 61% of the profile chord. This position corresponds to the average chordwise-placement of the spars in the reference aircraft ILR-01T.

The wingbox is assumed to be made of aluminum. The mechanical properties are summarized in **Table 4**.

Property	Value	Unit
Density	2700	kg/m^3
Elastic modulus	74	GPa
Yield strength ($\sigma_{0.2}$)	400	MPa

Table 4: *Material properties used for dimensioning*

Webs and caps are both assumed to carry shear and normal stresses. The cross section mechanic properties are described in Equation 3-6.

$$A = 2 \cdot (p_1 \cdot h + p_2 \cdot b) \tag{3}$$

$$I_c = 2 \cdot \left(\frac{h^3 \cdot p_1}{12} + p_2 \cdot b \cdot \left(\frac{h}{2}\right)^2\right) \tag{4}$$

$$I_n = 2 \cdot \left(\frac{b^3 \cdot p_2}{12} + p_1 \cdot h \cdot \left(\frac{b}{2}\right)^2\right) \tag{5}$$

$$I_T = \frac{2 \cdot (h \cdot b)^2}{\frac{b}{p_2} + \frac{h}{p_1}} \tag{6}$$

For each section, the sizing of the webs and caps can be described as an optimization problem where the linear density λ of each cross section has to be minimized.

$$\underset{p_1, p_2}{\text{minimize}} \quad \lambda = 2 \cdot \rho_{Al} \cdot (p_1 \cdot h + p_2 \cdot b)$$
$$\text{subject to:}$$
$$\sigma_v < \sigma_{0.2} \text{ at each point of the wingbox and}$$
$$p_1, p_2 > p\_min$$

The equivalent tensile stress σ_v is calculated with the von Mises yield criterion as shown in Equation 7.

$$\sigma_v = \sqrt{\sigma + 3 \cdot \tau^2} \tag{7}$$

The normal and shear stress are calculated using Equation 8-10. The total shear stress is calculated adding the

absolute values of the shear stress due to the torsion moment and the shear stress due to a shear force in n-direction. Shear stresses due to a force in c-direction are neglected.

$$\sigma = \frac{F_s}{A} + \frac{M_c}{I_c} \cdot n - \frac{M_n}{I_n} \cdot c \quad (8)$$

$$\tau_{Torsion} = \frac{M_s}{h \cdot b \cdot p_1} \quad (9)$$

$$\tau_{ShearForce} = \frac{3 \cdot b \cdot p_2 \cdot F_n}{2 \cdot h \cdot p_1 \cdot (h \cdot p_1 + 3 \cdot b \cdot p_2)} \quad (10)$$

Due to the rectangular geometry of the wingbox, the highest equivalent stress is present at one of the four corners. The coordinates of the critical corner can be calculated with Equation 11-12.

$$c_{CriticalPoint} = -sign(F_s) \cdot sign(M_n) \cdot \frac{b}{2} \quad (11)$$

$$n_{CriticalPoint} = sign(F_s) \cdot sign(M_c) \cdot \frac{h}{2} \quad (12)$$

The sizing itself is performed as a discrete optimization where both p_1 and p_2 can take values between 1 mm and 40 mm in 0.5 mm steps, as defined in Equation 13.

$$p_1, p_2 \in 1\ mm + 0.5\ mm \cdot k : k \in \mathbb{N}, k \leq 78 \quad (13)$$

Beginning at the lightest, all possible combinations of p_1 and p_2 are checked in ascending order, until one combination is found where the wingbox is able to withstand the calculated internal loads.

5. PYLON MODEL

The design of the pylon is essential for any podded engine configuration. MICADO calculates the pylon mass solely on the basis of the engine thrust, which is derived from existing engine and aircraft data. After placing the engines over the wing, the pylon geometry and its load carrying structure have to be readapted.

As a complex structural calculation cannot be carried out in the conceptual design stage, the pylon structure is modeled as a shear web structure. It serves the calculation of thin-walled structures, supported by rods. For the EoW pylon a parallelogram shear web structure is designed like presented in ***Figure 6***. The lower corners of the pylon are positioned along the wing chord at the front and rear spar positions. The engine is longitudinally centered between the upper corners. It is attached to the pylon at the height of a quarter of the nacelle's maximum diameter.

To size the structure of the pylon, as shown in ***Figure 6***, engine thrust (T) and inertial loads (W_{Nac}) of the nacelle are reduced as forces and a couple (T_M) acting on the upper nodes of the shear web.

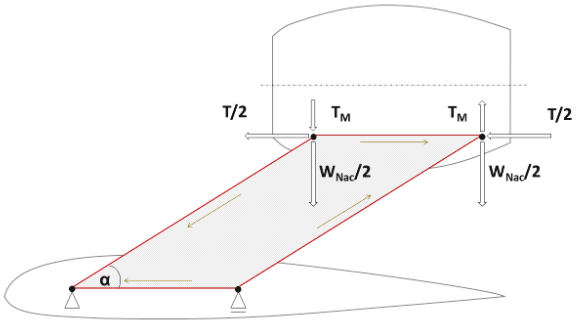

***Figure 6**: Structural pylon model with applied forces*

The pylon structure is assumed to be made of steel 4340, a frequently used steel in the aeronautic industry. With the material yield strength, the web thickness and the cross-section surface of the rods can be calculated considering the maximum stress in each rod and an additional safety factor of 1.5. Finally the volumes of web and rods are determined and multiplied with the density to obtain the masses.

To calibrate the model mass, the known mass of a real pylon installed at a specific engine and aircraft is used. Considering the same engine position a pylon mass is calculated with the structural model. The ratio of the real and calculated pylon mass f_{calib} describes the deviation between the structural model and the reality. Multiplying it with the calculated values delivers the final pylon mass.

$$f_{calib} = \frac{m_{P,real}}{m_{P,calc}} \quad (14)$$

The verification of the model is done by testing the thrust dependency of the resulting pylon masses. The empirical data for existing engines predicts an increase of pylon mass with increasing thrust, well approximated by the linear regression:

$$m_{P,MICADO} = 2.377 \cdot T + 233.29 \quad (15)$$

A comparison to the thrust induced change of the pylon mass calculated by the structural model is shown in **Figure 7**. The model pylon mass also grows with increasing thrust, as described in Equation 16. Thus the shear web model is applicable for a conceptual mass estimation of EoW pylons.

$$m_{P,model} = 2.2243 \cdot T + 212.99 \quad (16)$$

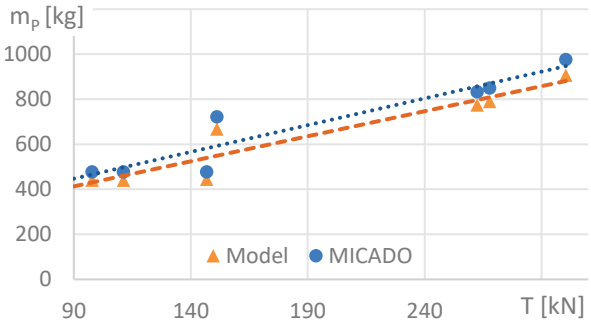

***Figure 7**: Pylon mass in relation to thrust calculated by MICADO and by the structural model*

6. PARAMETER STUDIES

The investigation of the over-the-wing engine positioning consists of three steps. First a fixed engine position over the wing is set while the wing geometry is varied. Afterwards the engine position is varied in order to reveal the dependencies of the correction factors on the chordwise, spanwise and vertical placement for the same wing geometry. Finally the impact on the overall aircraft design is investigated by using the calculated correction factors for a specified over-the-wing engine position within the MICADO design loop.

6.1. Wing parameter study

Three wing parameters are varied: the half span *b/2*, the chord length at kink position c_k and the leading edge sweep angle φ.

The relations of the wing mass and the drag coefficient are observed for discrete values of these parameters. The pylon mass is not taken into account here, since the pylon geometry does not change due to the fixed engine position relative to the wing. As an example the wing mass and the drag coefficient of EuW and EoW configuration are plotted for different kink chord values in Figures 8 and 9.

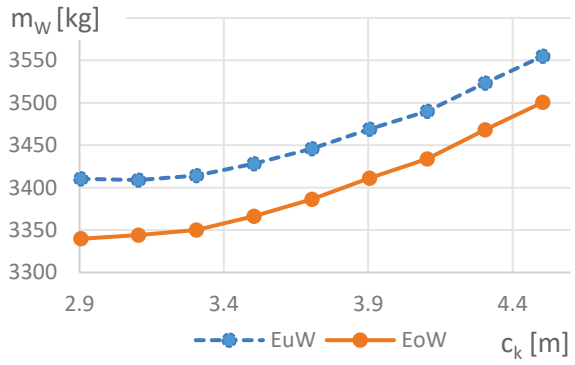

***Figure 8**: Wing mass of EuW and EoW in relation to kink chord length*

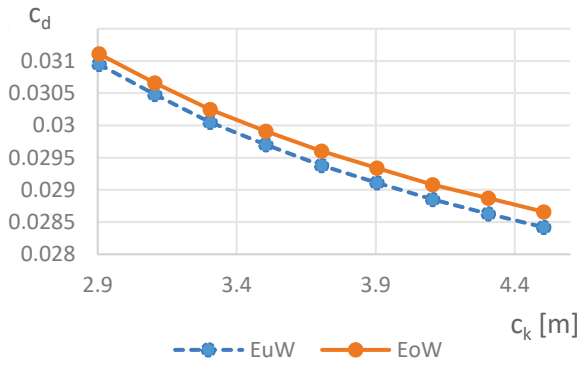

***Figure 9**: Drag coefficient of EuW and EoW in relation to kink chord length*

It can be observed that the curve slopes for EuW and EoW can be considered as identical. The wing mass and drag coefficient differences are approximately constant. This means that engines positioned over-the-wing are affected in the same way from wing parameter changes as engines under the wing. The assertion is confirmed by the maximum difference Δ_w and Δ_{Cd} of the correction factors for different chord lengths, which is negligible:

$$\Delta_W = \max(f_W) - \min(f_W) = 0.0054 \quad (17)$$

$$\Delta_{Cd} = \max(f_{Cd}) - \min(f_{Cd}) = 0.0033 \quad (18)$$

The same procedure was applied to the half span and the leading edge sweep. The maximum differences were under 2% in all investigations. These results indicate that there is no considerable difference in the impact of the wing geometry caused by the engine position.

6.2. Engine position variation

The effects of an over-the-wing engine placement depend on the exact position of the nacelle and cannot be generalized for all positions. To investigate this positioning effects, the nacelle is moved systematically chordwise, spanwise and normal to the wing. While varying one direction the position in the other two directions remain constant in a defined reference position.
The analysis is carried out for the three load cases shown in Table 5. Load cases LC1 and LC2 are used to determine the wing mass. Load case LC3 is the level flight at cruise condition, which is required to calculate the drag coefficient.

Parameter	Unit	LC1	LC2	LC3
Ma	-	0.78	0.31	0.78
H	m	10000	450	10000
n	-	2.5	2.5	1
v_{TAS}	m/s	233.58	106.089	233.58
T	kN	21.7	117.9	21.7

***Table 5**: Defined load cases*

The correction factors f_{WP} and f_{Cd} are derived using the methodology described in Section 3. That way the change in wing and pylon mass and in drag coefficient for placing the engines over the wing is indicated with respect to the T-tail aircraft with engines under the wing ILR-01T.

6.2.1. Chordwise variation

The chordwise nacelle position *x* over the wing is related to the chord length *c* and is varied between 0% (leading edge) and 100% (trailing edge) of the chord. In Figure 10 the combined mass coefficient is shown. The curves of the pure wing mass and the drag coefficient were also analyzed, but are not explicitly presented in this paper.

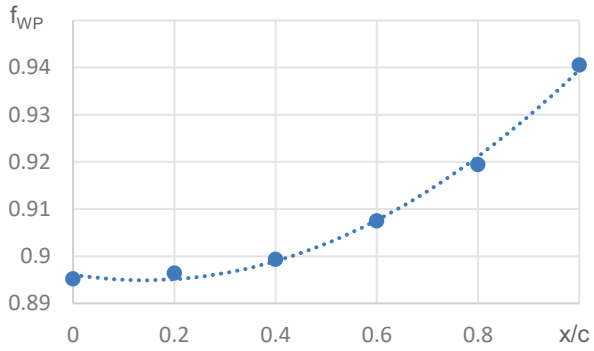

***Figure 10:** Mass factor for relative chordwise positions*

Although the factor for the pure wing mass has a maximum at a relative chord length of 40% the mass factor f_{wp} including pylon mass increases linearly for more backward positions of the nacelle. This is caused by a heavier pylon structure for a nacelle placed at the trailing edge. As the pylon model introduced in Section 5 is attached to the front

and rear spar, the parallelogram is stretched with a sharper angle leading to higher stress. Thus the combined mass does not decrease for backward positioned engines, like it is the case for the pure wing mass. The drag coefficient maximizes for a placement at 60% chord length. An over the wing position at the leading edge results in a lower c_D than for the reference EuW.
The equations describing the chordwise change of the drag coefficient and the structural mass are:

(19) $$f_{Cd}\left(\frac{x}{c}\right) = -0.0178 \cdot \left(\frac{x}{c}\right)^2 + 0.0213 \cdot \frac{x}{c} + 0.9987$$

(20) $$f_{WP}\left(\frac{x}{c}\right) = 0.0605 \cdot \left(\frac{x}{c}\right)^2 - 0.0171 \cdot \frac{x}{c} + 0.8961$$

According to the results a nacelle position at the leading edge would be favourable, due to lower mass and drag. However, this assumption is only valid for nacelles modelled as empty cylinders. As the ASDT model does not consider the exhaust of the engine and its effects on the wing, the drag coefficient does not represent the correct aerodynamics for forward engine positions. The exhaust flow is expected to disturb the airflow on the upper wing surface and thus worsening the aerodynamics. Regardless of the structural or aerodynamic effects, the chordwise engine position is determining the characteristics of the noise shielding. According to the placement at the trailing or leading edge, fan or jet noise can be shielded more effectively. This has to be considered in the design, since noise shielding is the main reason for using an EoW configuration

6.2.2. Spanwise variation

The spanwise engine positioning *y* is referenced to the half span *b/2* and varies between 20% and 50%. Figure 11 shows the correction factor for combined mass in relation to the half span position.

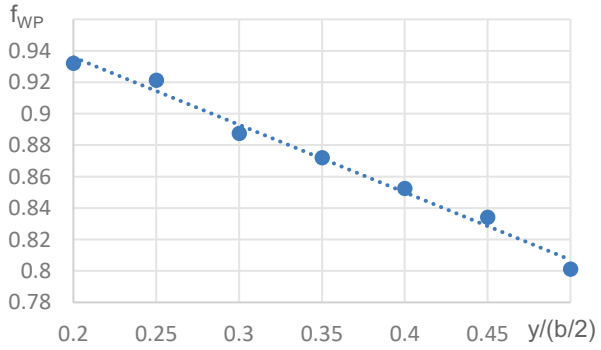

Figure 11: *Mass factor for relative spanwise positions*

The decreasing mass for a more outboard nacelle position is caused by the effect of bending moment relief explained. Outboard placed engines create a bigger negative bending moment in the wing root neutralizing the lift bending. As the wing surface is smaller for outer span positions and more lift is produced at the inner span with bigger surface, lower disturbance of the overall wing aerodynamics is the case for outboard placed engines. This additionally leads to a decrease of drag for engine positions towards the tips.
These effects are described in the equations for the correction factors in relation to the span position.

(21) $$f_{Cd}\left(\frac{y}{b/2}\right) = -0.0258 \cdot \frac{y}{b/2} + 1.011$$

(22) $$f_{WP}\left(\frac{y}{b/2}\right) = -0.4294 \cdot \frac{y}{b/2} + 1.0218$$

Given the fact that the mass and drag decrease for outer nacelle positions, it makes sense to place it as close to the tip as possible. However, the spanwise positioning is limited by the requirement of engine failure. With only one engine operating the aircraft must be controllable, which is not possible for the high moment caused by the lever of a tip ward positioned engine. Therefore a compromise between performance and controllability has to be found for the y-position.

6.2.3. Vertical variation

Different z-positions are realized by varying the vertical gap *h* between wing upper surface and the nacelles outside. It is defined in percentage of the outer nacelle diameter D_{out}. The height variation is done within the limits of 0% and 100% nacelle diameter shown in Figure 12. For the lower limit this means the nacelle is placed directly on the wing surface. Placing the engine at this height is not possible with a podded configuration. A buried integration would rather make sense. However the investigation of such an integration type is not possible with the given tools. Nevertheless this nacelle position can be revealing for aerodynamic analysis.

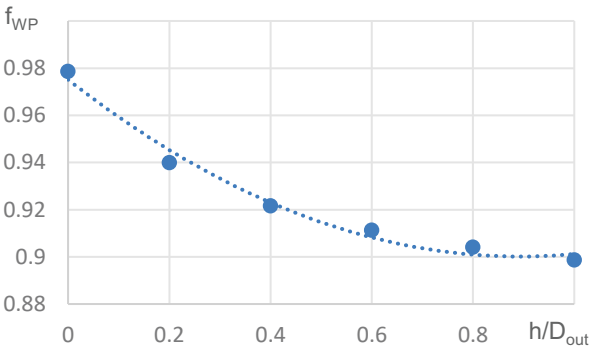

Figure 12: *Mass factor for relative vertical positions*

The pure wing mass declines approximately linear for a higher vertical nacelle position. This is caused by the higher moment due to the longer lever of the thrust axis. Such as an increase of thrust, it causes a higher nose-down moment on the wing. This is reducing the torsion on the box spar and thus decreasing its mass. Including the pylon mass, the structural mass decrease is quadratic as shown in Figure 11 and described in Equation 23. The drag coefficient decreases at higher nacelle positions due to lower disturbance of the wing airflow. Equation 24 describes this relationship for the drag coefficient correction factors.

(23) $$f_{Cd}\left(\frac{h}{D_{out}}\right) = 0.0019 \cdot \left(\frac{h}{D_{out}}\right)^2 - 0.0074 \cdot \frac{h}{D_{out}} + 1.0079$$

(24) $$f_{WP}\left(\frac{h}{D_{out}}\right) = 0.0849 \cdot \left(\frac{h}{D_{out}}\right)^2 - 0.1589 \cdot \frac{h}{D_{out}} + 0.9747$$

Summing up the results of the z-coordinate variation it is

better to place the engine as high as possible in aspects of mass as well as aerodynamics. This assumption is only valid for a static model, not considering aeroelastics and other dynamic effects. Also the reaction of the pylon mass for setting the nacelle higher is only correct for the applied simple model. It is highly questionable if a doubling in pylon length can result in a lighter pylon in reality. Therefore the nacelle should be placed with a maximum distance of 60% nacelle diameter to the wing surface, taking into account the diminishing aerodynamical benefit for higher positions.

6.3. Effects on overall aircraft

It is known from Section 2 that the influence of a varied engine position is not limited to the wing mass and drag coefficient. Primarily affecting the wing, the EoW configuration entails changes in the whole aircraft due to the interconnection of all components and systems. The results of this effect called snowball effect will be analyzed here as a last step of the aircraft performance investigation.

6.3.1. Engine position and correction factors

Due to the importance of the chordwise engine position for the noise shielding characteristic and the differences occurring in structural strain for its variation, two EoW positionings are investigated. In one configuration the engine is placed close to the trailing edge (ILR-01EoW-TE), while it is close to the leading edge in the other configuration (ILR-01EoW-LE).

As shown in Section 6.1 the correction factors are independent of the wing parameters and can be assumed constant. For the ILR-01EoW-TE and the ILR-01EoW-LE the factors describing the change of structural mass and drag coefficient relative to the ILR-01T are determined with Equations (1) and (2). Since the calculations of the wing and the pylon structure base on simple static models, a safety factor k have to be used to consider aeroelastic effects. Multiplying k with the structural mass correction factor f_{WP} results in the correction factor $f_{WP,k}$, which considers aeroelasticity.

$$f_{WP,k} = k \cdot f_{WP} \tag{25}$$

In this work a 25% mass growth due to aeroelastic effects is assumed, as for example flutter can stress the structure significantly. Therefore f_{WP} is multiplied with $k = 1.25$. For future calculations this safety factor has to be adapted according to researches done on the aeroelasticity of EoW configurations.
The obtained correction factors are summarized in Table 6.

$f_{Cd,LE}$	$f_{WP,k,LE}$	$f_{Cd,TE}$	$f_{WP,k,TE}$
1.0006	1.1205	1.0060	1.1519

***Table 6**: Correction factors for ILR-01EoW-TE and ILR-01EoW-LE*

These factors guarantee a mass estimation to the safe side for the EoW aircraft. The combined mass consisting of wing and pylon grows 10.23% for the ILR-01EoW-LE and 16.96% for ILR-01EoW-TE. Regarding this factors a better aircraft performance is expected with the ILR-01EoW-LE configuration.

6.3.2. Snowball effect analysis

In Table 7 the aerodynamic coefficients at cruise point and optimal lift-to-drag ratio are shown for the reference aircraft and the two EoW models. The design cruise point in MICADO is at 35000 feet with a Mach number of Ma_{cr} = 0.78 and a Reynolds number of $Re_{cr} = 25.6 \cdot 10^6$. It is seen that the snowball effect leads to decreasing total drag coefficients for both EoW configurations, although the correction factors provided a minimal increase. The lower total drag is caused by smaller induced and wave drag coefficients. Hence, the growth of viscous drag does not affect the total drag. The decrease in total drag coefficient is higher than for the lift coefficient, leading to better lift-to-drag ratios for the EoW configurations.

Parameter	ILR-01T	ILR-01EoW-LE	ILR-01EoW-TE
L/D_{opt}	17.81	18.05	18.09
$C_{l,opt}$	0.53	0.526	0.524
$C_{D,tot}$	0.02976	0.02914	0.02896
$C_{D,ind}$	0.01178	0.01126	0.011
% of tot	39.6	38.7	38
$C_{D,vis}$	0.01667	0.01667	0.01681
% of tot	56	57.2	58
$C_{D,wav}$	0.00131	0.00121	0.00115
% of tot	4.4	4.1	4

***Table 7**: Aerodynamic coefficients of ILR-01T, ILR-01EoW-TE and ILR-01EoW-LE*

It can be seen in Table 8 that the wing mass in MICADO changes about the amount predicted with the correction factors in Section 6.3.1. The absolute differences between the wing masses of the EoW and the reference EuW aircraft are 647kg for ILR-01EoW-LE and 1063kg for ILR-01EoW-TE. This equals an increase of wing mass by 10.16% and 16.7% respectively. Comparing the values with the direct change rates described by the mass correction factors before, the difference is under 1%. This indicates that no considerable snowball effect occurs for the wing mass itself. Though the snowball effect leads to a total structural mass addition of 706kg and 1151kg. This is mainly added through the landing gear and the pylon mass. For the ILR-01EoW-LE the OWE increases by 2.02%due to the higher structure and power unit mass, while the MTOW increase of 1.23% is lower. The mass difference between OWE and MTOW consists of the payload and the fuel. Since the TLARs and thus the payload and range remain the same for all aircraft, this difference equals the loaded fuel. The fuel mass calculated for the design mission is also presented in Table 8. Due to higher additional structure mass and higher OWE, the mass growth of ILR-01EoW-TE is bigger than of ILR-01EoW-LE. Thus, also more fuel is needed for this configuration. Nevertheless both EoW aircraft have to carry extra fuel as a result of their increased OWE.

Comp.	Unit	ILR-01T	ILR-01EoW-LE	ILR-01EoW-TE
MTOW	**kg**	**73502**	**74610**	**74870**
OWE	kg	42476	43468	43696
MWE	kg	38160	39152	39381
Structure	**kg**	**20780**	**21609**	**21810**
Wing	kg	6365	7126	7315
Fuselage	kg	9790	9790	9790
Hor. tail	kg	708	708	709
Ver. tail	kg	504	505	505
L. Gear	kg	2371	2409	2418
Pylons	kg	1043	1071	1073
Power Unit	**kg**	**7854**	**8065**	**8083**
Systems	**kg**	**5412**	**5361**	**5370**
Fuel	**kg**	**16024**	**16152**	**16186**

***Table 8**: Mass breakdown of ILR-01T, ILR-01EoW-LE and ILR-01EoW-TE*

The change in pylon mass indicates that the thrust used for the different aircraft models is not the same, as MICADO calculates the pylon mass based on the engine thrust. A comparison of the engine data in Table 9 reveals the differences in cruise and maximum thrust. For higher thrust MICADO automatically sizes up the engine dimensions including the mass. This explains the increase in power unit mass for the EoW configurations.

Parameter	Unit	ILR-01T	ILR-01EoW-LE	ILR-01EoW-TE
Engine Width	m	1.83	1.88	1.88
Engine Height	m	2.12	2.17	2.18
Engine Length	m	2.52	2.57	2.58
Cruise Thrust	kN	22.1	23.1	23.2
Maximum Thrust	kN	120	125.9	126.3
Engine and Nacelle Mass	kg	7444	7670	7687

***Table 9**: Engine data of ILR-01T, ILR-01EoW-LE and ILR-01EoW-TE*

The empennage geometry and positioning is exactly the same for the two EoW configurations and the EuW reference. Since the wing geometry and positioning remains the same, the lever arm of the tail also is unaffected. The results are not plausible, regarding the differences in aerodynamics and mass, the gravity centers have to change. Thus, with a constant wing, the tail size has to be adapted.

The results of the snowball effect must be viewed critically as many of the effects of over-the-wing engines particularly on the components besides the wing are not considered. For example, the landing gear mass is calculated in MICADO based on the MTOW and does not take into account, that it could be made shorter for EoW aircraft. Also, the pylon mass calculation has to be adapted to the EoW configuration with the structural model introduced in Section 5. Another point is the dimensioning of the empennage by MICADO, which is not calculated plausibly. Consequently possible changes in the tail mass are not measured accurately. Considering these points the snowball effect would produce different results.

7. CONCLUSION AND OUTLOOK

According to the results shown in the preceding section, the position of over-the-wing engines can influence the mass of the wing by more than 15%. For the considered load cases, placing the engine in outboard, fore and high positions relative to the reference configuration decreases the structural mass. Outboard engine positions decrease the bending moment in the wing, fore positions decrease the pylon mass and high positions decrease the nacelle's aerodynamic influence on the wing, improving its drag coefficient.

Examining the overall effects on the aircraft, EoW seem to result in higher masses than their EuW counterparts. Through the snowball effect component masses beside the wing increase, leading to higher OWE and thus more fuel burn. However, a more detailed analysis should be performed to get more realistic results. Taking into account both transonic and aeroelastic effects while doing aerodynamic calculations and sizing the structure would improve the quality of the results. When considering the whole aircraft, further factors as landing gear, pylon and empennage design should be considered and integrated into the design loop.

References

[1] Airbus, “Global Market Forecast: Growing Horizons 2017/2036,” 2017.

[2] Bertsch, L., *Noise Prediction Noise Prediction within Conceptual Aircraft Design*, Braunschweig, Germany, 2013.

[3] Lieber, L., Brown, D., and Golub, R. A., *Small Engine Technology (SET) Task 23 ANOPP Noise Prediction for Small Engines, Wing Reflection Code*, Phoenix, AZ United States, 2000.

[4] Lieber, L., and Golub, R., *Small Engine Technology (SET) - Task 13 ANOPP Noise Prediction for Small Engines: Jet Noise Prediction Module, Wing Shielding Module, and System Studies Results*, Phoenix, AZ United States, 2000.

[5] Stone, J. R., Krejsa, E. A., and Clark, B. J., “Jet Noise Modeling for Coannular Nozzles Including the Effects of Chevrons,” 2003, https://ntrs.nasa.gov/search.jsp?R=20030093553.

[6] Krejsa, E. A., and Stone, J. R., *Enhanced Fan Noise Modeling for Turbofan Engines*, Cleveland, OH United States, 2014.

[7] Bloomer, H. E., “Investigation of wing shielding effects on CTOL engine noise,” 1979, https://ntrs.nasa.gov/search.jsp?R=19790044957.

[8] Dobrzynski, W., Ewert, R., Pott-Pollenske, M., Herr, M., and Delfs, J., “Research at DLR towards airframe noise prediction and reduction,” *Aerospace Science and Technology*; Vol. 12, No. 1, 2008, pp. 80-90. doi: 10.1016/j.ast.2007.10.014.

[9] Kinney, D., Hahn, A., and Gelhausen, P., “Comparison of low and high nacelle subsonic transport configurations,” *15th Applied Aerodynamics Conference*, 1997. doi: 10.2514/6.1997-2318.

[10] Peter Jeschke, “Luftfahrtantriebe I und II,” RWTH Aachen University, 2012.

[11] Raymer, D. P., *Aircraft design. A conceptual approach,* 5th edn., AIAA American Inst. of Aeronautics and Astronautics, Reston, Va., 2012.

[12] Fujino, M., and Kawamura, Y., “Wave-Drag Characteristics of an Over-the-Wing Nacelle Business-Jet Configuration,” *Journal of Aircraft*; Vol. 40, No. 6, 2003.

[13] Wright, J. R., and Cooper, J. E., *Introduction to aircraft aeroelasticity and loads*, John Wiley, Chichester, 2007.

[14] Fujino, M., Oyama, H., and Omotani, H., “Flutter Characteristics of an Over-the-Wing Engine Mount Business-Jet Configuration,” *44th AIAA/ASME/ASCE/AHS/ASC Structures 2003*, 2003. doi: 10.2514/6.2003-1942.

[15] Fujino, M., “Design and Development of the HondaJet,” *Journal of Aircraft*; Vol. 42, No. 3, 2005, pp. 755-764. doi: 10.2514/1.12268.

[16] Fujino, M., “HondaJet; Case Study 4,” *AIAA* [online], 2011, https://www.hondajet.com/Content/pdf/tech_papers/NC_vol%202_CS4_HondaJet_Kym15May.pdf.

[17] Risse, K., Anton, E., Lammering, T., Franz, K., and Hoernschemeyer, R., “An Integrated Environment for Preliminary Aircraft Design and Optimization,” *53rd AIAA/ASME/ASCE/AHS/ASC Structures, Structural Dynamics and Materials Conference*, AIAA 2012-1675, AIAA, 2012.

[18] Franz, K., Lammering, T., Risse, K., Anton, E., and Hörnschemeyer, R., “Economics of Laminar Aircraft Considering Off-Design Performance,” *53rd AIAA/ASME/ASCE/AHS/ASC Structures, Structural Dynamics and Materials Conference*, AIAA 2012-1760, AIAA, 2012.

[19] Lammering, T., Anton, E., Risse, K., Franz, K., and Hörnschemeyer, R., “Influence of Off-Design Performance on the Design of Aircraft with Laminar Flow Technology,” *11th AIAA Aviation Technology, Integration, and Operations (ATIO) Conference*, AIAA 2011-7017, 2011.

[20] Pereda Albarrán, M. Y., Schueltke, F., and Stumpf, E., “Sound Quality Assessments of Over-the-Wing Engine Configurations Applied to Continuous Descent Approaches,” *AIAA Aviation, 25-29 June 2018, Hyatt Regency Atlanta, Atlanta, Georgia*, 2018.

[21] Anton, E., Lammering, T., and Henke, R., “A comparative analysis of operations towards fuel efficiency in civil aviation,” *RAeS Aerodynamics Conference 2010 [electronic resource],* Royal Aeronautical Society, London, 2010.

[22] Horstmann, K.-H., Engelbrecht, T., and Liersch, C. M., “LIFTING_LINE: Version 2.3,” 2010.

[23] Teichmann, M., *Bestimmung der Strukturmasse nicht konventioneller Flügelsysteme mit Hilfe eines erweiterten FEM-Flügelbalkenmodells*, 2013.

[24] CeRAS, “Central Reference Aircraft data System,” http://ceras.ilr.rwth-aachen.de.

[25] Risse, K., Schäfer, K., Schültke, F., and Stumpf, E., “Central Reference Aircraft data System (CeRAS) for research community,” *CEAS Aeronautical Journal*; Vol. 7, No. 1, 2016, pp. 121-133. doi: 10.1007/s13272-015-0177-9.

[26] Raymer, D. P., *Aircraft design: A conceptual approach. AIAA Education Series*, AIAA, Washington, DC, 1992.

[27] Chambers, M. C., Ardema, M. D., Patron, A. P., Hahn, A. S., Miura, H., and Moore, M. D., “Analytical Fuselage and Wing Weight Estimation of Transport Aircraft,” 1996, https://ntrs.nasa.gov/search.jsp?R=19960025262.

[28] Cavagna, L., Ricci, S., and Travaglini, L., “NeoCASS: An Integrated Tool for Structural Sizing, Aeroelastic Analysis and MDO at Conceptual Design Level,” 2013, p. 1025. doi: 10.2514/6.2010-8241.

[29] Drela, M., and Youngren, H., “AVL 3.36 User Primer,” 2017.]